for the average cheilostome species to generate a progressively greater skeletal mass than the average cyclostome species. This could result from a gradual trend toward relatively larger colony sizes within cheilostomes (*17*), a greater number of colonies per cheilostome species, or both.

These data suggest that multiple measures of biotic change through time are necessary for a rich understanding of biospheric evolution. As in contemporary biotic communities, taxonomic diversity captures only limited aspects of the complexity of the biota (*18*). Multiple measures of biotic systems provide greater insight into history and processes and a better basis for predicting future biodiversity.

Reference and Notes

1. P. W. Signor, *Annu. Rev. Ecol. Syst.* **21**, 509 (1990); J. J. Sepkoski Jr., *Paleobiology* **19**, 43 (1993); in *Global Events and Event Stratigraphy in the Phanerozoic*, O. H. Walliser, Ed. (Springer-Verlag, Berlin, 1995), pp. 35–51; M. J. Benton, *Science* **268**, 52 (1995).
2. J. J. Sepkoski Jr. and M. L. Hulver, in *Phanerozoic Diversity Patterns*, J. W. Valentine, Ed. (Princeton Univ. Press, Princeton, NJ, 1985), pp. 11–39.
3. W. I. Ausich and D. J. Bottjer, *Science* **216**, 173 (1982); G. J. Vermeij, *Evolution and Escalation* (Princeton Univ. Press, Princeton, NJ, 1987); J. J. Sepkoski Jr., *Paleobiology* **14**, 221 (1988); R. K. Bambach, *ibid.* **19**, 372 (1993).
4. C. W. Thayer, in *Biotic Interactions in Recent and Fossil Benthic Communities*, M. J. S. Tevesz and P. O. McCall, Eds. (Plenum, New York, 1983), pp. 480–625.
5. Counts of individuals are inappropriate for skeletalized colonial organisms because of modularity and fragmentation, and the sizes of sexually mature bryozoan colonies range over several orders of magnitude. Therefore, skeletal mass was taken as an appropriate proxy for abundance or biomass [W. I. Ausich, *Ohio J. Sci.* **81**, 268 (1981); G. Staff, E. N. Powell, R. J. Stanton Jr., H. Cummins, *Lethaia* **18**, 209 (1985)]. We stress that this proxy is potentially subject to taphonomic bias and is strictly empirical. Competitive dominance in the once-living community requires different bases of inference.
6. S. J. McNaughton and L. L. Wolf, *Science* **167**, 131 (1970); R. H. Whittaker, *Communities and Ecosystems* (Macmillan, New York, ed. 2, 1975); J. H. Brown and B. A. Maurer, *Nature* **324**, 248 (1986); E. O. Wilson, *The Diversity of Life* (Belknap, Cambridge, MA, 1992).
7. J. B. C. Jackson, *Paleobiology* **14**, 307 (1988); S. L. Wing, L. J. Hickey, C. C. Swisher, *Nature* **363**, 342 (1993); M. L. Droser, D. J. Bottjer, P. M. Sheehan, *Geology* **25**, 167 (1997).
8. T. L. Phillips and R. A. Peppers, *Int. J. Coal Geol.* **3**, 205 (1984); D. W. Krause, *Univ. Wyoming Contrib. Geol. Spec. Pap. 3* (1986), pp. 95–117; S. Lidgard and J. B. C. Jackson, *Paleobiology* **15**, 255 (1989); B. E. Berglund, H. J. B. Birks, M. Ralska-Jasiewiczowa, H. E. Wright, Eds., *Paleoecological Events During the Last 15,000 Years* (Wiley, Chichester, UK, 1996); R. Lupia, P. R. Crane, S. Lidgard, in *Biotic Response to Global Change: The Last 145 Million Years*, S. J. Culver and P. F. Rawson, Eds. (Chapman & Hall, London, in press).
9. F. K. McKinney and J. B. C. Jackson, *Bryozoan Evolution* (Unwin Hyman, Boston, 1989).
10. P. D. Taylor and G. P. Larwood, in *Extinction and Survival in the Fossil Record*, G. P. Larwood, Ed. (Clarendon, Oxford, 1988), pp. 99–119.
11. All bryozoan fragments retained on 0.5-mm and larger screens were picked from 60 entire disaggregated 0.3- to 3.0-kg samples or, where bryozoans were extraordinarily abundant, from subsamples; fragments were sorted on the basis of clade, and total mass for each clade was determined directly or calculated on the basis of subsamples. Species that produce colony fragments typically smaller than 0.5 mm have not been included in most previous studies of bryozoan species diversity [summarized in (*13*)]. We have excluded such small size fragments from our calculations of relative skeletal mass as well; these fractions are subject to winnowing in many recent bryozoan habitats and are rarely derived from the ecologically dominant taxa. Nonetheless, small colonies of cyclostomes and cheilostomes may be numerous in some environments (E. Håkansson, personal communication). Our data were supplemented by data in O. Berthelsen, *Danmarks Geol. Unders.* **83**, 1 (1962) and A. H. Cheetham, *Smithsonian Contrib. Paleobiol.* **6**, 1 (1971). Some variation in the data inevitably results from variable amounts of cement or of matrix or shell fragments. Cyclostomes tend to have thinner walls than do cheilostomes, and raw cheilostome mass was weighted by 1.26 on the basis of a thin-section determination of the ratio of skeleton to cement plus adherent material in control samples [33 cheilostomes ($\bar{X}$ = 0.62, SD = 0.147) and 35 cyclostomes ($\bar{X}$ = 0.51, SD = 0.151) from four representative collections]. Additional "noise" in the data may be due to different taphonomic responses of cyclostome and cheilostome bryozoans in different environments. However, dissolution and abrasion rates of mineralized bryozoans are dependent upon diverse factors that cut across clade assignment [A. M. Smith, C. S. Nelson, P. J. Danaher, *Palaeogeogr. Palaeoclimatol. Palaeoecol.* **93**, 213 (1992); A. M. Smith and C. S. Nelson, in *Biology and Palaeobiology of Bryozoans*, P. J. Hayward, J. S. Ryland, P. D. Taylor, Eds. (Olsen & Olsen, Fredensborg, Denmark, 1994), pp. 177–180; in *Bryozoans in Space and Time*, D. P. Gordon, A. M. Smith, J. A. Grant-Mackie, Eds. (National Institute of Water & Atmospheric Research Ltd., Wellington, New Zealand, 1996), pp. 213–226.
12. J. J. Sepkoski Jr., *J. Paleontol.* **71**, 533 (1997).
13. S. Lidgard, F. K. McKinney, P. D. Taylor, *Paleobiology* **19**, 352 (1993).
14. The skeletal mass of cyclostomes was 70% in middle Danian and 62% in late Danian.
15. G. R. Upchurch, in *Mass Extinctions Process and Evidence*, S. K. Donovan, Ed. (Columbia Univ. Press, New York, 1989), pp. 195–216; S. J. Fowell and P. E. Olsen, *Tectonophysics* **222**, 361 (1993); R. P. Speijer and G. J. Van der Zwan, in *Biotic Recovery from Mass Extinction Events*, M. B. Hart, Ed. (The Geological Society, London, 1996), pp. 343–371.
16. M. Foote, *Palaeontology* **34**, 461 (1991); *Univ. Michigan Mus. Paleontol. Contrib.* **28**, 101 (1991); *Proc. Natl. Acad. Sci. U.S.A.* **89**, 7325 (1992); *Paleobiology* **19**, 185 (1993); *ibid.* **21**, 273 (1995); *Science* **274**, 1492 (1996).
17. The mean size of encrusting cyclostomes is 4.7 mm^2 and of cheilostomes is 10.1 mm^2 on shell debris in the Mainstreet Limestone Member of the Grayson Formation (Albian), Roanoke, Texas; the mean size of encrusting cyclostomes is 5.8 mm^2 and of encrusting cheilostomes is 51.8 mm^2 on shell debris in the northern Adriatic off Rovinj, Croatia (F. K. McKinney, unpublished data). The two faunas are qualitatively judged to represent colony size of contemporaneous faunas, and the major change has been an increase in mean size of cheilostome colonies.
18. K. J. Gaston, Ed., *Biodiversity: A Biology of Numbers and Difference* (Blackwell, Oxford, 1996).
19. L. Wilkinson, *SYSTAT: The System for Statistics* (Systat, Evanston, IL, 1990).

20. Supported by the NSF (DEB 9306729 to S.L.; EAR 9117289 to F.K.M.), U.S.-U.K. Fulbright program (F.K.M.), National Geographic Society (F.K.M.), Petroleum Research Fund of American Chemical Society (F.K.M.), NASA (NAGW-1963 to J.J.S.J.), and Global Change and the Biosphere Programme of the National History Museum/University College London (P.D.T.). We thank S. Hageman, R. Lupia, and two anonymous reviewers for evaluating the manuscript and numerous colleagues who served as guides to field localities.

16 April 1998; accepted 26 June 1998

In Situ Observations of a High-Pressure Phase of H_2O Ice

I-Ming Chou,* Jennifer G. Blank,† Alexander F. Goncharov, Ho-kwang Mao, Russell J. Hemley

A previously unknown solid phase of H_2O has been identified by its peculiar growth patterns, distinct pressure-temperature melting relations, and vibrational Raman spectra. Morphologies of ice crystals and their pressure-temperature melting relations were directly observed in a hydrothermal diamond-anvil cell for H_2O bulk densities between 1203 and 1257 kilograms per cubic meter at temperatures between −10° and 50°C. Under these conditions, four different ice forms were observed to melt: two stable phases, ice V and ice VI, and two metastable phases, ice IV and the new ice phase. The Raman spectra and crystal morphology are consistent with a disordered anisotropic structure with some similarities to ice VI.

The manifold ways in which the water molecules may link through hydrogen bonding give rise to a remarkably rich phase diagram (*1–5*). Enhancing this complexity is the existence of both proton-ordered and -disordered forms as well as metastable crystalline and amorphous phases (*3, 6*). Though evidence for additional phases in the system has been obtained in the past [for example, (*7*)], information about them has been very sparse, if not controversial, because previous studies have relied principally on quench techniques or limited in situ probes (*7–10*). Here we document the existence of another H_2O phase from in situ microscopy and Raman spectroscopy at 0.7 to 1.2 GPa. The phase exhibits an

I. Chou, 955 National Center, U.S. Geological Survey, Reston, VA 20192, USA. J. G. Blank, A. F. Goncharov, H. Mao, R. J. Hemley, Geophysical Laboratory and Center for High Pressure Research, Carnegie Institution of Washington, 5251 Broad Branch Road, NW, Washington, DC 20015, USA.

*To whom correspondence should be addressed.
†Present address: Department of Geology and Geophysics, University of California, Berkeley, CA 94720, USA.

unusual crystalline morphology and shows evidence of significant proton disorder.

Five liquidus phases of ice have been documented to 2 GPa; four are stable phases (ices Ih, III, V, and VI) and one is metastable (ice IV) (*11*). The pressure-temperature (*P-T*) melting relations of these phases are shown in Fig. 1. These phases, including both stable and metastable variants, are evident by their distinct melting curves (*7, 8, 10*). Ice IV was inferred by Bridgman (*2*), and was subsequently confirmed to be a metastable phase that formed in the stability fields of ice V (*8*) and ice VI (*12*). Evidence of metastable phases was also reported in the vicinity of the ice V stability field (*7*). Kamb (*13*) predicted the structures of additional phases on the basis of the symmetries of the known phases. Recently, a metastable phase was reported below 0.6 GPa (*14*) and two phases were suggested at higher pressures (to ~1.2 GPa) (*15*), indicating that much remains to be learned about H_2O in this *P-T* region.

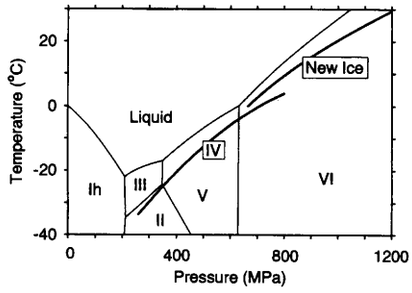

Fig. 1. Phase diagram of H_2O. The boundaries for the stable phases (thin lines) are from (*26*). The heavy lines are melting curves for ice IV (*12*) and the new phase (this study). The melting of ice VII occurs at much higher *P-T* conditions. The maximum estimated uncertainties in the calculated pressures at the T_m of ice V and VI were less than ±3%.

We used a hydrothermal-type diamond-anvil cell (*16*) to study the phase diagram and physical properties of ices in the complex region of the phase diagram below 2 GPa. For preparation of a sample, a drop of distilled deionized H_2O is loaded in the sample chamber of the cell (a hole of ~500 μm in diameter in a 125-μm-thick Re gasket sandwiched between two diamond anvil faces). After the sample chamber is sealed, the total mass of H_2O remains constant, and the density of the water ρ can therefore be adjusted by compressing the diamond anvils and changing the volume of the sample chamber. Once the volume of the sample chamber is fixed, the sample remains under isochoric conditions; thermal expansion of various parts of the cell, within the small temperature range of this study, has a negligible effect on the sample volume.

Typically, the water sample froze at about −40°C (and ~600 to 800 MPa), and well-formed crystals (Fig. 2) could be grown by slow cooling right before the individual ice grains melted (*17*). Under isochoric conditions with bulk sample densities between 1203 and 1257 kg/m^3, up to three different forms of ice were observed to melt: ice V, ice VI, and an ice that could not be ascribed to a known phase. We suggest that this marks a new solid phase of H_2O (Table 1). We occasionally observed ice IV (*12*). For each measured melting temperature T_m of ices V and VI, we calculated the corresponding pressure and water density from available data (*18, 19*). The pressure at the melting temperature of the new phase was then calculated [with the equation of state of water (*19*)] from the

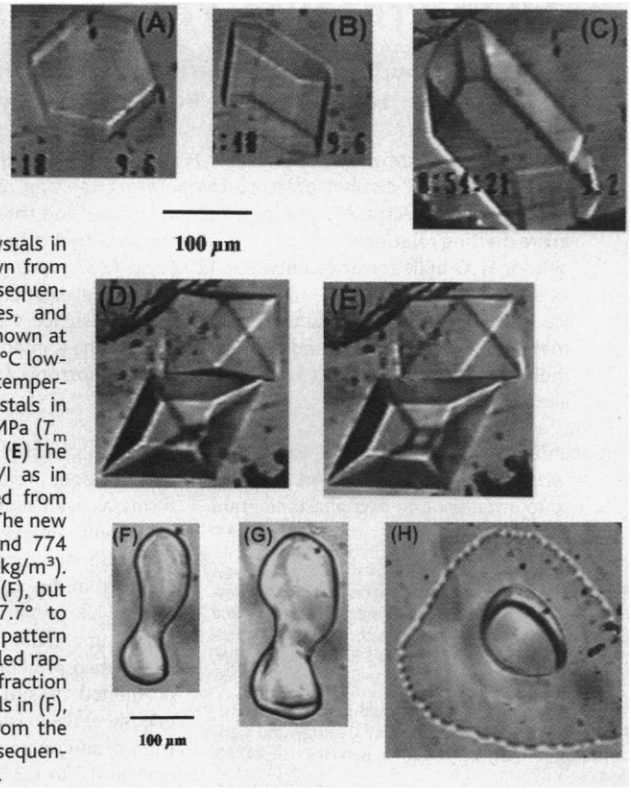

Fig. 2. Morphologies and growth patterns of ice V (panels A, B, and C), ice VI (panels D and E), and the new phase (panels F, G, and H). (**A** and **B**) Ice V in water at 9.8°C and 855 MPa (T_m = 10.1°C; density ρ = 1226 kg/m^3). (**C**) Ice V in water at 9.4°C and 845 MPa. The ice V crystals in (A), (B), and (C) were grown from the same crystallite seed in sequential warming-cooling cycles, and the temperature readings shown at lower right corners were 0.2°C lower than the respective true temperatures. (**D**) Two ice VI crystals in water at 40.9°C and 1241 MPa (T_m = 42.6°C; ρ = 1268 kg/m^3). (**E**) The same two crystals of ice VI as in (D), but which were cooled from 40.9° to 40.3°C in 29 s. (**F**) The new phase in water at 7.7°C and 774 MPa (T_m = 8.1°C; ρ = 1212 kg/m^3). (**G**) The same crystal as in (F), but which was cooled from 7.7° to 7.0°C in 9 s. (**H**) The growth pattern of the new phase when cooled rapidly from 7.9° to 7.2°C in a fraction of a second. Note the crystals in (F), (G), and (H) were grown from the same crystallite nucleus in sequential warming-cooling cycles.

Table 1. The measured melting temperatures of ice polymorphs (T_m, in degrees Celsius) and the calculated pressures (P_m, in megapascals) and water densities (ρ, in kilograms per cubic meter) at the melting points. Dashes indicate not determined.

New phase			Ice V		Ice VI	
T_m	ρ*	P_m†	T_m	P_m‡	T_m	P_m‡
		Experiment 1				
21.4	–	(1000)	14.1	974		
21.4	1245	1023			30.7	1059
		Experiment 2				
9.4	1220	821	8.3	817		
9.6	1221	831	8.7	827		
9.6	1218	812			16.2	836
		Experiment 3				
12.3	1223	852	9.2	840		
14.2	1228	886	10.4	871		
16.5	–	(925)	11.9	909		
16.5	1231	918			23.5	944
17.1	–	(927)	11.9	909		
17.1	1231	920			23.5	944
26.3	1257	1131			37.4	1176
26.4	1257	1132			37.4	1176
		Experiment 4				
11.6	1222	840	8.8	830		
11.6	1220	830			17.2	850
		Experiment 5				
3.0	1203	702	3.5	704		
3.0	1203	706	3.7	708		
5.3	1207	733	4.7	731		
5.3	1207	735	4.8	733		
8.8	1216	796	7.2	790		
9.4	1216	798	7.2	790		
		Experiment 6				
9.3	1215	793	7.0	785		
9.3	1215	793			14.4	811
		Experiment 7				
4.7	1205	723	4.3	722		
		Experiment 8				
6.2	1210	752	5.5	749		
		Experiment 9				
15.5	1230	908			23.0	936
15.5	1229	901			22.4	927
		Experiment 10				
8.1	1213	779	6.5	773		
8.1	1212	775			13.0	792

* Under the isochoric condition of the experiment, these densities were calculated from the melting *P-T* conditions of either ice V or ice VI by using the equation of state of water (*19*). † Calculated from T_m and density by using the equation of state of water (*19*). Numbers in parentheses are estimated values and were not used in regression for the melting curve; their *P-T* conditions exceed the extrapolation range of (*19*). ‡ Calculated from T_m with the equations given in (*18*).

density obtained for the isochoric melting of ice V or ice VI (*20*).

Different polymorphs of ice can be identified by their distinct crystal morphologies, growth patterns (Fig. 2), and melting curves (Fig. 3). The *P-T* melting relations for the new phase can be represented by the equation P (MPa) = 665.1 (±9.1) + 12.73 (±1.15)T + 0.184 (±0.039)T^2, over the temperature interval $0 < T < 30$°C (a least squares fit to the data listed in Table 1). The new phase has poor crystallinity in our experiments; the crystals are birefringent (*21*). The growth patterns and melting *P-T* relations of the new phase indicate that this phase is definitely not ices Ih, III, IV, V, and VI.

To characterize further the new solid phase of H_2O, we obtained low- and high-frequency Raman spectra of the low-temperature phases of ice, including measurements as a function of temperature (Fig. 4). Taken together, these spectra provide fingerprints for each of the phases and confirm identification by crystal morphology. The new phase exhibits bands in the lower frequency region at 192 cm^{-1} and 490 cm^{-1} (for example, at the reference temperature of −30°C); these are assigned to translational and rotational (librational) excitations. In the higher frequency (O–H stretching) region, a sharper feature at 3215 cm^{-1} and shoulder at 3410 cm^{-1} were observed. The structure in this spectral region is distinct from that of the other ice phases. The lack of sharp structure in the low-frequency translational and rotational excitations indicates that protons (or molecular orientations) are disordered in this new ice, as found for ices Ih, V, and VII. The spectra show that the new phase is distinct from both low and high density amorphous ice (*6, 22*). The low- and high-frequency bands are similar to those measured for ice VI (and ice III), but the additional structure at lower frequency (bands at 145 and 157 cm^{-1} in ice VI) is absent (*23*). The presence of such modes is a strong indicator of partial proton order.

We propose that the new ice phase described here is a disordered phase having a density similar to that of ice VI (*24*). The possible structural link between the new phase and ice VI is indicated by the observation that ice VI crystallized during rapid isochoric cooling of the water sample immediately after melting of the new phase. Although the morphology suggests an amorphous phase, the Raman spectra and birefringence indicate the presence of long-range order and structural anisotropy. The locking-in of states of order and disorder to produce new metastable phases may be a general feature of ices in this complex region of the phase diagram. Unusual shifts observed in the melting curves of ices III and V have also been interpreted as arising from the formation of various degrees of proton order and disorder (*25*). The new phase may also be related to ice VI in the way that disordered ice VII is related to ordered ice VIII. A better analogy may be to ices VII and VII′ formed by pressure-induced crystallization of high-density amorphous ice (*6*). Theoretical study of these states of order and disorder should lead to improved understanding of water and hydrogen bonding in chemical, geological, and biological systems.

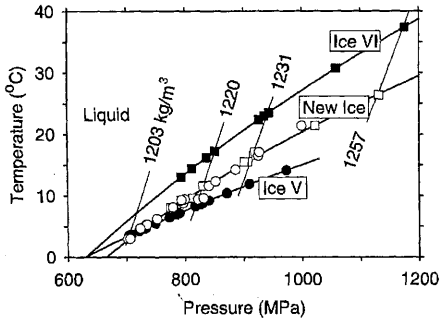

Fig. 3. The *P-T* melting relations of ice V (solid circles), ice VI (solid squares), and the new ice phase (open circles and squares derived from water densities based on the melting of ice V and ice VI, respectively). Plotted are the data from Table 1. Also shown are four isochores (labeled by density) of water. The melting curves for ice V and ice VI are from (*18*). The melting curve for the new ice phase is described by the equation given in the text.

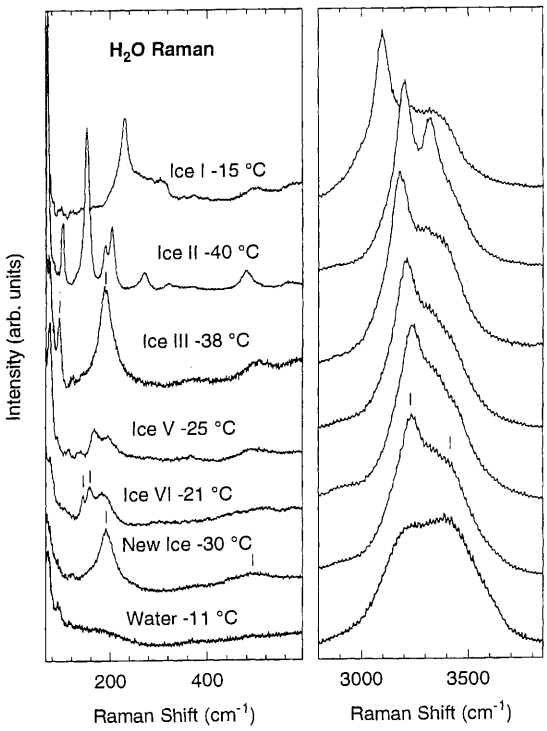

Fig. 4. Raman spectra of the new ice phase compared with ices I, II, III, V, VI, and water measured in situ in the diamond cell. Ice I is proton disordered; ice II is proton ordered; ice III is partially proton disordered but has a proton-ordered form (ice IX); ice V is partially proton disordered. We suggest that ice VI is partially ordered as well. The spectrum of supercooled water is in good agreement with previous work [for example (*27*)]. Weak peaks <100 cm^{-1} in that spectrum arise from spurious scattering. The tick marks denote characteristic Raman peaks discussed in the text: bands at 192, 490, 3215, and 3410 cm^{-1} for the new phase; 145 and 157 cm^{-1} for ice VI; and 95 and 190 cm^{-1} for ice III. Intensity is given in arbitrary units. Detailed analysis of the spectra of the additional phases will be presented elsewhere.

References and Notes

1. G. Tammann, *Ann. Phys.* **2**, 1 (1900).
2. P. W. Bridgman, *Proc. Am. Acad. Art Sci.* **47**, 441 (1912).
3. O. Mishima, L. D. Calvert, E. Whalley, *Nature* **310**, 393 (1984); *ibid.* **314**, 76 (1985); O. Mishima, *ibid.* **384**, 546 (1996).
4. P. H. Poole, F. Sciortino, U. Essman, H. E. Stanley, *Nature* **360**, 324 (1992). S. Harrington, R. Zhang, P. H. Poole, F. Sciortino, H. E. Stanley, *Phys. Rev. Lett.* **78**, 2409 (1997).
5. A. F. Goncharov, V. V. Struzhkin, M. Somayazulu, R. J. Hemley, H. K. Mao, *Science* **273**, 218 (1996). K. Aoki, H. Yamawaki, M. Sakashita, H. Fujihisa, *Phys. Rev. B* **54**, 15673 (1996).
6. R. J. Hemley, L. C. Chen, H. K. Mao, *Nature* **338**, 638 (1989).
7. H. Englehardt and E. Whalley, *J. Chem. Phys.* **56**, 2678 (1972).
8. P. W. Bridgman, *ibid.* **3**, 597 (1935).
9. T. B. Bizhigitov and N. N. Sirota, *JETP Lett.* **44**, 417 (1986).
10. L. F. Evans, *J. Appl. Phys.* **38**, 4930 (1967).
11. P. V. Hobbs, *Ice Physics* (Clarendon Press, Oxford, 1974). See, for example, figure 1.19.
12. I. M. Chou and H. T. Haselton Jr., *Rev. High Press. Sci. Tech.* **7**, 1132 (1998).
13. B. Kamb, in *Physics and Chemistry of Ice,* E. Whalley, S. J. Jones, L. W. Gold, Eds. (Royal Society of Canada, Ottawa, 1973), pp. 28–41.
14. C. Lobban, J. L. Finney, W. F. Kuhs, *Nature* **391**, 268 (1998).
15. O. Mishima and H. E. Stanley, *Rev. High Press. Sci. Tech.* **7**, 1103 (1998).
16. W. A. Bassett, A. H. Shen, M. Bucknum, I. M. Chou, *Rev. Sci. Instr.* **64**, 2340 (1993).
17. The sample was cooled by a stream of cold nitrogen and heated by two individual heaters, and the sample temperatures were detected by two K-type thermocouples in direct contact with the diamonds; for the reported temperatures, the precision is ±0.1°C and accuracy is ±0.5°C. The images of the sample under a microscope, together with the temperature and time information, were recorded continuously on videotape.
18. W. Wagner, A. Saul, A. Pruss, *J. Phys. Chem. Ref. Data* **23**, 515 (1994).
19. A. Saul and W. Wagner, *ibid.* **18**, 1537 (1989).
20. For example, for experiment 10 (Table 1), observations were made at a fixed bulk water density, and the new phase, ice V, and ice VI were observed to melt at 8.1°, 6.5°, and 13.0°C, respectively. The bulk

water density calculated from T_m of ice VI is 1212 kg/m^3, which yielded a pressure of 775 MPa at T_m = 8.1°C; a pressure of 779 MPa was obtained when we assumed that the bulk water density was 1213 kg/m^3 (on the basis of the melting point of ice V). The two calculated pressures for the melting of the new phase at 8.1°C agree. Similar results were also obtained for other melting temperatures (Fig. 3) even under more extreme *P-T* conditions where uncertainties are involved in extrapolating both the melting curve of ice V (*18*) and the equation of state of water (*19*).

21. A quantitative determination of the birefringence cannot be made because samples were viewed between the two diamonds, the tips of which become birefringent under stress.
22. T. C. Sivakumar and S. A. Rice, *J. Chem. Phys.* **69**, 3468 (1978); D. D. Klug, O. Mishima, E. Whalley, *ibid.* **86**, 5323 (1987). These amorphous forms are reportedly stable only at lower temperatures.
23. The lowest frequency band sharpened somewhat with decreasing temperature, but no new peaks appeared. This observation, together with weak frequency shifts, indicates that the phase did not become significantly more ordered with cooling. The 192 cm^{-1} band and the structure of spectrum in the O–H stretching region are also similar to that measured for ice III; however, the latter also has a characteristic band at 95 cm^{-1}, which was not observed for the new phase.
24. Kamb (*13*) proposed that pressure-quenched ice VI is partially ordered with space group *Pmmn*. In its stability field, the phase is proton-disordered (space group $P4_2/nmc$) and a fully ordered form (space group *Pn*) was also predicted (*13*). Subsequent study by W. L. Kuhs, J. L. Finney, C. Vettier, and D. V. Bliss [*J. Chem. Phys.* **81**, 3612 (1984)] confirmed that the space group of ice VI is $P4_2/nmc$. Our results indicate that the new phase is more extensively disordered. Because of the lack of data, it is difficult to speculate the relation, if any, between the new phase and the one recently found at lower pressures by Lobban *et al.* (*14*).
25. I. M. Chou, in *Workshop on Hydrogen Bonds at High Pressure* (Japan Science and Technology Corporation, Gifu, Japan, 21 to 23 August 1997), p. 11.
26. H. T. Haselton Jr., I. M. Chou, A. H. Shen, W. A. Bassett, *Am. Mineral.* **80**, 1302 (1995).
27. G. D'Arrigo, G. Maisano, F. Mallemace, P. Migliardo, F. Wanderlingh, *J. Chem. Phys.* **75**, 4264 (1981). R. Bansil, J. Wiafe-Akenten, J. L. Taaffe, *ibid.* **76**, 2221 (1982); Y. Yeh, J. H. Bilgram, W. Kanzig, *ibid.* **77**, 2317 (1982).
28. We thank W. A. Bassett, H. T. Haselton Jr., E. Karmon, and V. V. Struzhkin for assistance with experiments, and P. B. Barton Jr. and R. R. Seal for reviews. Supported by the U.S. Geological Survey (Deep Continental Studies Program), NSF (D.M.R. and E.A.R.), and NASA.

13 March 1998; accepted 15 June 1998

Evidence Against a Significant Younger Dryas Cooling Event in New Zealand

Christiane Singer, James Shulmeister,* Bill McLea

Pollen records of deglacial sequences from northwest Nelson, New Zealand, demonstrate that there was no significant temperature decline associated with the Younger Dryas in New Zealand. Records of glacial advances at this time were either the product of increased snow accumulation under enhanced precipitation regimes or random variation rather than the result of a regional thermal decline. This finding supports those models of Younger Dryas initiation that require neither enhanced westerly circulation nor significant thermal decline in the Southern Hemisphere.

The Younger Dryas (YD) was a brief but intense climatic deterioration that occurred 11,000 to 10,000 radiocarbon years before the present (B.P.), during the termination of the last glaciation. The New Zealand record of YD is crucial to understanding the phenomenon on a global scale, as only New Zealand and Chile and Argentina possess mid-latitude glaciers in the Southern Hemisphere that are likely to be sensitive to atmospheric cooling, and the South American record has proved inconclusive and contradictory (*1–3*). In New Zealand, a significant advance of the Franz Josef Glacier in Westland has been dated to YD times (*4*). Although the dating (*5, 6*) and the interpretation that the advance relates to thermal decline (*7*) are controversial, the record has been widely cited (*8–10*) as evidence of the interhemispheric influence of the event.

Supporting evidence of cooling in the New Zealand region during the YD has been elusive. Some other glacial advances in the Southern Alps may be coeval, but adequate dating control is lacking; where dated sequences of deglacial ages do occur, there is no concentration of ages in the YD Chron (*11, 12*). The other primary source of climate data from New Zealand are pollen studies, but these have consistently shown a pattern of ongoing afforestation from 14,000 to 10,000 radiocarbon years B.P. This is interpreted as a stepwise warming with no trend reversals (*13*); however, only a few sites covered the YD Chron in detail, and there were no sites near the glaciers. We present a pollen record, from a climatically sensitive site, that covers the YD.

The Cobb Valley in northwest Nelson lies about 300 km north of the Franz Josef Glacier (Fig. 1), close to the west coast of the South Island. It has the same regional climate as Westland. The mountains of northwest Nelson were less extensively glaciated than the main ranges of the Southern Alps, because they are at lower elevations, but small piedmont caps and widespread valley glaciation occurred. Terminal and lateral moraines, roche moutonée fields, and other evidence of valley glaciation are present in the Cobb Valley and on a plateau north of the valley. Associated with the terminal moraine complexes are a series of kettle holes formed by the melting out of large blocks of stagnant ice. These kettles have subsequently infilled with lake sediments and peats. The oldest of these kettles started filling soon after the Last Glacial Maximum (LGM; ~18,000 radiocarbon years B.P.), and it is almost certain that a valley glacier still occupied the lower Cobb Valley during the deglaciation.

We obtained three pollen records (Fig. 2) from different kettle holes that extend back beyond the YD. All three records show consistent trends. At full glacial times, the residual vegetation in the Cobb consisted of grasses, daisies, other herbs, and low shrubs (Fig. 2A). Rapid revegetation occurred 13,000 radiocarbon years B.P. [(*12*) and Fig. 2C], and the herbaceous flora was replaced by a low shrubland dominated by *Phyllocladus* (a dwarf podocarp). Soon thereafter another montane podocarp, *Halocarpus*, and a *Nothofagus* (southern beech)—represented by fuscasporites-type pollen, probably mountain beech (*N. solandri* var *cliffortiodes*)—expanded. At all sites, the dominant vegetation associations until after 10,000 radiocarbon years B.P. comprised mixes of these taxa. *Halocarpus* and *N. solandri* gradu-

Table 1. Radiocarbon dates from Cobb Valley and adjoining areas.

Code	Age* (conventional)	Age† (calibrated)	Core (depth in meters)	Material	Notes
NZA7771	3,511 ± 72	3,870–3,643	CV1 (0.98)	Peat	Arrival of silver beech
NZA8032	9,991 ± 76	11,630–11,005	CV1 (1.93)	Peat	Termination of YD
NZA6325	11,195 ± 95	13,214–13,000	CV1 (2.06)	Peat	Onset of YD
NZA7198	13,200 ± 85	15,904–15,578	LS1 (2.95)	Rootlets	Onset of postglacial flora
NZA8033	17,120 ± 100	20,531–20,048	CV3 (3.91)	Fine organics	LGM

*Age in conventional radiocarbon years B.P. †Calibrated age range in years B.P. (*19*).

Research School of Earth Sciences, Victoria University, Post Office Box 600, Wellington, New Zealand.

*To whom correspondence should be addressed. E-mail: james.shulmeister@vuw.ac.nz